Solar Energy Materials & Solar Cells 251 (2023) 112109

Contents lists available at ScienceDirect

Solar Energy Materials and Solar Cells

journal homepage: www.elsevier.com/locate/solmat

# Setting the baseline for the modelling of Kesterite solar cells: The case study of tandem application

Alex Jimenez-Arguijo [a,b,c], Axel Gon Medaille [a,b,c], Alejandro Navarro-Güell [a,b], Maykel Jimenez-Guerra [a,b], Kunal J. Tiwari [a,b,c], Marcel Placidi [a,b,c], Moleko Samuel Mkehlane [d], Emmanuel Iwuoha [d], Alejandro Perez-Rodriguez [c,e], Edgardo Saucedo [a,b], Sergio Giraldo [a,b], Zacharie Jehl Li-Kao [a,b,*]

[a] Universitat Politècnica de Catalunya (UPC), Photovoltaic Lab – Micro and Nano Technologies Group (MNT), Electronic Engineering Department, EEBE, Av Eduard Maristany 10-14, Barcelona, 08019, Catalonia, Spain
[b] Universitat Politècnica de Catalunya (UPC), Barcelona Center for Multiscale Science & Engineering, Av Eduard Maristany 10-14, Barcelona, 08019, Catalonia, Spain
[c] Institut de Recerca en Energia de Catalunya (IREC), 1,2ªpl. Jardins de les Dones de Negre, 08930, Sant Adria de Besos, Barcelona, Spain
[d] Sensor Lab, Department of Chemistry, University of the Western Cape, Bellville, 7535, South Africa
[e] Departament d'Enginyeria Electrònica i Biomedica, IN2UB, Universitat de Barcelona, C/ Marti i Franques 1, Barcelona, 08028, Spain

ARTICLE INFO

*Keywords:*
Kesterite
Tandem solar cells
Modelling
Baseline
SCAPS

ABSTRACT

The Kesterite solar cells research landscape is at a crossroad and despite a much improved understanding of the limitations of this class of materials, the current performance deficit contrasts with the several other thin film technologies reaching conversion efficiency values well above 20%. It is more important than ever for the Kesterite community to collaborate directly or indirectly and data sharing is an essential building block in that regard. This work proposes a detailed set of modelling baselines and parameters, based on a consistent set of properties obtained with experimental devices made by our group. These parameters permit to accurately reproduce all photovoltaic figures of merits of reference experimental Kesterite cells with a relative accuracy of 1% or less. As a case study, and using optical modelling based on the transfer matrix method in complement, the potential of Kesterite materials in tandem devices with either a Perovskite or a Crystalline Silicon partner is evaluated. It is found that a moderate improvement of pure selenium CZTSe, feasible in the short to middle term, would realistically permit to use this material as bottom subcell in tandem with a Perovskite top cell and obtain efficiencies reaching the 30% threshold. On the other hand, using a Kesterite absorber in a top subcell with a silicon bottom subcell appears as particularly ambitious even when considering several important optimizations to the material, and it is believed that only an important breakthrough would render this material viable for such application. The complete set of material parameters, optical indices and modelling files are shared for the Kesterite community to use and build improve upon.

## 1. Introduction

Kesterite solar cells have graduated from the status of emerging chalcogenide material in the landscape of thin film photovoltaics (PV), with close to two decades of a research effort by the community. Yet, and despite a substantial effort in the last ten years, the technology has struggled to overcome its performance deficit as compared to other more mature materials such as CIG(S,Se) or CdTe, in a large part due to a bottleneck in open-circuit voltage ($V_{oc}$) which origin has remained highly debatable until recently. The Kesterite family of materials holds nevertheless several assets critical for a future-proof solar cell absorber, above all the absence of critical raw or toxic constituents, while combining the advantages of inorganic thin films such as stability, bandgap tunability, lightweightness, and mechanical flexibility, all of which are strong points in the perspective of emerging PV applications (building integrated PV, Internet of Things etc.).

In the meantime, the understanding of the $V_{oc}$ deficit in Kesterite-based solar cells has recently progressed thanks to breakthroughs in

* Corresponding author. Universitat Politècnica de Catalunya (UPC), Photovoltaic Lab – Micro and Nano Technologies Group (MNT), Electronic Engineering Department, EEBE, Av Eduard Maristany 10-14, Barcelona, 08019, Catalonia, Spain.
*E-mail address:* zacharie.jehl@upc.edu (Z. Jehl Li-Kao).

https://doi.org/10.1016/j.solmat.2022.112109
Received 4 October 2022; Received in revised form 5 November 2022; Accepted 14 November 2022
Available online 29 November 2022

materials modelling [1,2] and this limitation was ascribed in large part to the existence of native point defects such as, for example, $Sn_{Zn}$ in CZTSe. Following these advances, recent experimental results [3–6] with new record values suggest that we could be entering a new, higher performance era for Kesterite. In the meantime, crystalline silicon (c-Si) devices have become nearly ubiquitous in the landscape of standard PV production owing the numerous advantages of silicon, and the next step for the PV industry lies in affordable devices with efficiencies beyond the detailed balance limit of single junction, that is ≳30%. Tandem architectures are currently the only concept with experimentally proven performance exceeding that threshold, and the rise of Perovskite throughout the last decade has allowed for Perovskite/c-Si tandems to recently reach such landmark value [7]. In the meantime, both CIGSe and CdTe have achieved efficiencies well above 20% [8,9] and represent credible alternatives as bottom cell and top cell respectively. In that context, it is crucial for Kesterite to catch up in terms of performance within this decade, and very encouraging results for Perovskite/Kesterite tandems were recently obtained [10].

The modelling of complete devices is instrumental in both predicting the outcome of a specific optimization, and in the interpretation of experimental results. However, the often simple models used to investigate a specific aspect of the device usually lead to qualitative rather than quantitative results, and achieving a semblance of quantitative assessment remains challenging in the absence of an exhaustive representation of the device. Furthermore, as finding materials properties can be challenging for research groups without access to performant devices, it is often necessary to rely on educated guesswork or on various and possibly inconsistent sources coming from the characterization of materials with different deposition processes, which can in return affect the conclusions even at a qualitative level; the prime example being how bandgap grading and back surface field have been for long hailed as a critical strategy in Kesterite based on modelling work, while the experimental results are yet to deliver any significant advancement beyond the state of the art. A recently published study [11] illustrates the necessity of curated data when modelling thin film solar cells. This paper claims the feasibility of Perovskite/Kesterite tandem devices with efficiencies well beyond 30%. However, and despite relying on simulations made using a program with advanced functionalities such as COMSOL, the set of baseline data does not represent the reality of state of the art devices nor their possible future optimization, resulting in unrealistic results, with for instance a Kesterite cell performing higher than the Perovskite cell under AM 1.5 illumination (24.76% vs 22.85% respectively, with a surprising and likely unattainable 87% Fill Factor for the Kesterite cell). Similarly, another study recently published on a similar topic [12] reports highly unrealistic calculated figures of merit due to the lack of a solid reference. Rather than focusing on advanced modelling tools, our work argues for the necessity of a realistic and consistent set of baseline parameters using simpler modelling tools, for both accurate quantitative modelling and realistic qualitative observations. Using the widely known SCAPS program [13], our work proposes baselines for Kesterite-based solar cells, made readily available to the community, using a consistent set of data characterized on our champion devices for both narrow bandgap Kesterite (pure Se-CZTSe) and wide bandgap Kesterite (pure S-CZTS) [14,15]. The quantitivity of the baselines is assessed against experimental results, displaying a high degree of realism. Establishing such baseline is arguably the main objective of this work, not unlike what was previously done for CIGSe and CdTe by Gloeckler et al. in Ref. [16]. A case study relevant to the Kesterite community on the potential of these materials for tandem devices, both as top subcell (with c-Si bottom cell) and bottom subcell (with Perovskite top cell), is carried out, using a transfer matrix method approach to model the optical part which is decoupled from the electrical modelling by SCAPS. Interestingly, it is found that a moderate increase of the efficiency of CZTSe solar cell up to 15–16% (AM 1.5), primarily achieved by reducing the bulk defect density ($Sn_{Zn}$ and [$Sn_{Zn}$ + $Cu_{Zn}$] for CZTSe and CZTS respectively), would render this material viable as bottom cell assuming a Perovskite top cell performing in the 21–22% ballpark with a total tandem efficiency approaching or equaling the detailed balance limit of a single junction. On the other hand, using a wide bandgap Kesterite absorber in a top subcell combined with a state of the art c-Si bottom subcell appears extremely challenging, as even a full set of optimizations leads to performance barely reaching that of usual high performing single junction cells such as CIGSe, CdTe or c-Si. It is therefore obvious that wide bandgap Kesterite needs a significant breakthrough not accounted here to become viable in the tandem PV landscape, while the narrow bandgap Kesterite counterpart appears to have a more streamlined pathway to become a relevant solution as bottom subcell.

The conclusions obtained on tandem devices set realistic expectations for the community working on applying Kesterite materials in tandem devices, and offer quantitative insights in Kesterite-based solar cells as a whole by evaluating the potential performance improvements of some of the leading research pathways. Beyond those important results, the goal of this work is to offer a common framework for the Kesterite community to build upon when using numerical modelling to evaluate solar cells, and particularly for groups with a limited capacity to produce or characterize experimental samples. By offering a consistent set of parameters and sharing all data and readily useable ".scaps" files as supplementary information, we hope to contribute improving the quality of future works of the community when using modelling, and hopefully encouraging a more systematic data sharing and peer assessment in the field of Kesterite solar cells research.

## 2. Materials and methods

This study aims at modelling in a quantitative manner Kesterite solar cells, and proposes the case study of tandem architecture with either a Perovskite cell (Kesterite bottom cell) or a c-Si cell (Kesterite top cell). In both cases, SCAPS 3.308 is used to model the electrical part [13], while the optical part is modelled using the transfer matrix approach with an in-lab developed custom code, similar to what is described in Ref. [17]. In each case, a four terminal architecture (4T) is considered, though a similar study could be carried out for a 2T design using a similar framework. A particular emphasis is made on sharing all data used in this work including both optical and electronic parameters. The set of optical data includes all optical indices used for the modelling of the devices' optical transmissivity, reflectivity and specific layer absorption. The community is encouraged to use the consistent set of data ($E_G$, hole concentration, electron affinity, thickness, …) embedded within the ".scaps" files in the supplementary information as a baseline for device modelling. Nevertheless, it is essential to assess the value and limitations of those data by possibly using them and hopefully improving upon those.

### 2.1. Perovskite/Kesterite tandem

When CZTSe Kesterite is in a bottom cell configuration, the optical transmission of a realistic Perovskite solar cell stack on transparent substrate and calculated by the transfer matrix method is input as optical filter in SCAPS. $FAPbI_3$ is used as absorber for the Perovskite top cell, and the material stack considered is similar to that reported in Ref. [18]: SLG/ITO/$TiO_2$/$FAPbI_3$/Spiro-OMeTAD/ITO. The thicknesses for each layer can be found in the supplementary information to this work Fig. S 1. The complex optical indices of all films constituting the Perovskite top cell are extracted from the following references [19–21].

The bottom CZTSe Kesterite cell is electrically modelled after the champion device reported by our group in Ref. [14], allowing for a consistent set of material (example: carrier concentration, mobility) and device (example: front reflectivity) parameters characterized on solar cells produced with a single, well-controlled process, which we believe is a key point in obtaining a realistic baseline. Nevertheless, the bulk defects' type and concentration remains challenging to experimentally

determine in a complex material such as Kesterite, and conflicting reports exist in that regard [2,22,23]. However, the recent work by Kim et al. [2] based on first principle calculation has offered a novel insight in the existence of defects limiting the performance of Kesterite devices. Importantly, the nature and main characteristics of the $Sn_{Zn}$ point defect was established. In this work, we thus consider the presence of a (2+/+) point defect with a 0.5 eV transition energy and a capture cross section $\sigma = 9.3 \times 10^{-14} cm^2$, corresponding to the values reported in the supplementary information of [2]. As the defect density depends on various external parameters such as the experimental conditions, this value was manually adjusted to a value $n = 8e14.cm^{-3}$ for which all four figures of merit ($V_{oc}$, $J_{sc}$, FF and efficiency) match those of our experimental cell under AM 1.5 illumination. It should be emphasized that the bulk defect density was the only relevant parameter being adjusted here, and having the four performance indicator simultaneously matched is a strong indication of the reliability of the model. Using this mimicry as a baseline, the device's performance in tandem conditions is evaluated, and various possible and realistic improvements are investigated. In each case, those are justified by an existing research line within the Kesterite community.

The electrical modelling of the Perovskite top cell is beyond the scope of this work, as the focus in on optimizing Kesterite specifically. In tandem configuration, the Kesterite performance is assessed and a target efficiency for the Perovskite top cell is given for the complete device to overcome the 30% efficiency threshold. This value is arbitrarily chosen as being close to the detailed balance limit of a single junction.

### 2.2. Kesterite/c-Si tandem

The modelling of the wide bandgap Kesterite top cell, in combination with a c-Si bottom cell, follows a similar approach although in this case, a state-of-the-art c-Si bottom cell is also electrically modelled. The simulation of the c-Si cell is made using the baseline device provided by default in SCAPS, with some minor modifications made based on the experience of our group with c-Si cells. With a calculated AM 1.5 efficiency of 22.9%, this cell is intended to be a realistic representation of a typical high efficiency c-Si photoconverter.

The Kesterite top cell is electrically modelled based on our sulfur-CZTS champion device fabricated on transparent $SnO_2$:F (FTO) substrate and reported in Ref. [15], using a consistent set of material parameters. Bulk defects' parameters are again extracted from the supplementary information found in Ref. [2], with a (0/+) point defect having a 0.9 eV transition energy and a capture cross section $\sigma = 1.5 \times 10^{-13}\ cm^2$ corresponding to the [$Sn_{Zn}$-$Cu_{Zn}$] cluster point defect. Additionally, interface defects are added following the recent work described in Ref. [24], and are found preponderant in this work. To assess the tandem efficiency, the wide $E_g$ Kesterite top cell is optically modelled and the resulting transmission is used as input to determine the performance of the c-Si bottom cell in tandem condition. It should be noted that unlike our experimental reference, where an ultrathin layer ($\approx$ 20 *nm*) of $MoS_2$ was used between the Kesterite and the FTO back contact, we consider an $MoO_3$ interlayer (= 20 *nm*) in the optical modelling as our recent results suggest that it is much more suited for transparency purpose [25]; from an optical viewpoint, the Kesterite top cell can thus be considered well-optimized. Contrary to the previous case of a Perovskite/Kesterite, the total tandem efficiency is here calculated as both top and bottom cell are electrically modelled in SCAPS.

## 3. Results and discussion

### 3.1. CZTSe as bottom subcell

#### 3.1.1. Setting the baseline

In this part of our work, we consider the feasibility of a tandem solar cell between a state-of-the-art Perovskite top cell and a pure Se, CZTSe solar cell with a bandgap of 1.04 eV. The top cell is optically modelled and the resulting optical transmission is used as an input for the optical and electrical modelling of the bottom CZTSe subcell. As described in the methodology part of this work, the quantitative modelling of Kesterite devices is the primary focus of this work, and we propose to use a target efficiency for the Perovskite cell, with the aim for the tandem device to overcome the single junction detailed balance limit of $\sim$ 30%: $\eta^{top}_{Pero} = 30 - \eta^{bottom}_{CZTSe}$.

Efficiencies of 25% can obtained with a Perovskite $FAPbI_3$ absorber of optical bandgap $E_g = 1.5\ eV$ [18]. In this work, the optical index of $FAPbI_3$ used for optical modelling was extracted from Ref. [19], and the bandgap was estimated from calculated transmission curves to be $E_g = 1.56\ eV$. While this value can already be considered wide enough to be used as top cell in a tandem architecture, wider bandgaps have been reported for this class of materials while retaining high efficiencies [26–29], with values up to 1.68 *eV*. We calculate in Fig. 1 the total optical transmission of the two possible perovskite solar cells configurations. The complete optical profile (reflectivity and layer specific absorption) can be found in the Supplementary Information Fig. S 2. As expected, an important number of photons can be gained using a 1.68 eV absorber, and the integration of the difference in optical transmission shows that a maximum value of 2.1 mA $cm^{-2}$ can be gained by the bottom cell, which represents about 10% in relative efficiency gain in tandem conditions. While the top cell's performance ought to be optimized first and foremost in a tandem device, there is a significant upside in widening the Perovskite bandgap as long as performance can be preserved.

Using a consistent set of experimental parameters is critical to quantitatively assess the potential of Kesterite cells in a tandem device. The modelling requires a baseline model which accurately reproduces a state-of-the-art experimental solar cell under AM 1.5 illumination condition. Hence, most of the materials parameters were experimentally determined on the champion cell produced by sputtering and reactive thermal annealing at our laboratory described in Ref. [14], ensuring a near perfect consistency. The bulk defect profile, which is known to be the main performance limitation for this class of absorber, remains however challenging to unequivocally assess. As mentioned previously, the $Sn_{Zn}$ defects properties reported in the supplementary information of [2] are used to parametrize Shockley-Read-Hall (SRH) recombination in

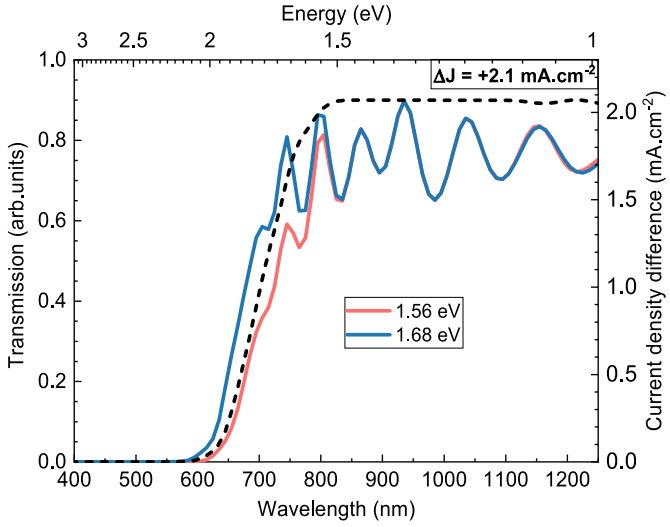


**Fig. 1.** Calculated optical transmissions of the following solar cell stack: SLG/ITO/$TiO_2$/$FAPbI_3$/Spiro-OMeTAD/ITO. The Perovskite bandgaps are 1.56eV (red line) and 1.68eV (blue line). The dotted line represents the maximum gain in current for the bottom cell calculated by integrating the difference between both transmissions. (For interpretation of the references to colour in this figure legend, the reader is referred to the Web version of this article.)

the bulk of the material. The reader might verify that the capture cross-sections of $Sn_{Zn}$ are the main factor limiting the $V_{oc}$ of Kesterite solar cells, even at low concentrations. By adjusting the defect density to 8E14 $cm^{-3}$, we are able to model a quantitative numerical mimicry of our champion cell with a remarkable accuracy, as illustrated Fig. 2. Indeed, a difference of less than 1% is obtained for each figure of merit such simultaneous level of agreement on all four PV parameters reinforces our confidence in the quantativity and reliability of the model. Therefore, we believe this baseline to be realistic enough to properly assess the potential of Kesterite absorbers in a tandem device, along with several experimentally realistic optimizations to help push the conversion efficiency beyond the single junction detailed balance limit. In the following, the 30% tandem efficiency threshold will be used as point of reference. The efficiency of the Kesterite bottom cell in tandem condition will be calculated, from which an efficiency target for the top Perovskite cell will be determined.

### 3.1.2. Tandem performance and incremental optimizations

When using the Perovskite top cell's transmission as optical input in combination to the aforementioned Kesterite baseline, the resulting bottom cell PV parameters in tandem conditions are calculated (Table 1) and the CZTSe efficiency is 4.1% and 5.6% for the 1.56 eV and the 1.68 eV Perovskite bandgaps respectively, which corresponds to a top cell efficiency target of 25.9% and 24.4% if one aims at a tandem overcoming the single junction detailed balance limit. While those values for the top cells appear within the realm of possible for an excellent Perovskite cell, the necessity to fabricate the top cell on a transparent substrate along with the target of a larger Perovskite bandgap renders efficiencies around 25% overly ambitious, and the Kesterite bottom cell ought to be improved.

As mentioned before, $Sn_{Zn}$ has been identified as the main performance bottleneck in Kesterite-based solar cells, and it was calculated that $3.2 \times 10^{14} cm^{-3}$ was the minimum achievable defect density in optimal growth conditions. [2]. Several strategies are currently being considered to address this limitation, among which small atom transient doping (H) is one of the most promising currently experimentally pursued by our group [4], and could theoretically lower the minimum achievable defect density. The first possible optimization to the CZTSe bottom consists in a lowering by one order of magnitude (OM) of the bulk defect density from $n = 8e14.cm^{-3}$ down to $n = 8e13.cm^{-3}$, as shown Table 1. While a 1 mA $cm^{-2}$ improvement in $J_{sc}$ is obtained, the most remarkable improvements are seen in the $V_{oc}$ and Fill Factor, which confirm that addressing the issue of $Sn_{Zn}$ would solve in large part the $V_{oc}$ deficit plaguing this technology. The resulting efficiency in subcell tandem conditions is improved by 2 points (absolute) and reaches 7.6% (14.4% in AM 1.5 conditions); this lowers the threshold efficiency for a 30% tandem to 22.4% for the Perovskite subcell, a value challenging on transparent substrate but well within reach of the ever-growing Perovskite community. The passivation of interface defects by one OM does not markedly improve performance, an expected result as the spike band offset between CdS and CZTSe permits to alleviate the influence of interface defects. Finally, as the reduction in bulk defect density leads to an increase of the carrier diffusion length, it becomes relevant to address the issue of back interface recombination, even more so as in subcell tandem configuration, most photons are red and infrared with a larger absorption depth. The addition of a linear, 500 nm back surface field (BSF), which was experimentally reported by our group through a composition grading in Germanium [30], yields a real yet limited subcell efficiency improvement up to 8.1%, corresponding to a 21.9% efficiency target for the Perovskite top cell if aiming for a 30% tandem. It should be stressed that the conversion efficiency of the CZTSe cell under AM1.5 illumination would be, in this configuration, 15.4%. A value below most of the claimed short term objectives for this technology, and only 1.8 points above the current and recently improved state of the art [3,5]. However, our model also reveals that without first addressing the issue of carrier diffusion length by reducing the bulk defect density, a back grading/BSF has very little use as carriers do not diffuse that deep in the absorber; this specific observation explains why bandgap grading strategies have failed so far to deliver performance enhancements beyond the state of the art in Kesterite devices, despite past modelling reports pointing such strategy as essential [31,32]. For comparison purpose, we also propose the case of perfectly selective front and back contacts, using adjusted work functions for both electrodes. No improvement is observed compared to the previous case, which indicates that contacts are not a limitation and that even by reducing the bulk defect density by one OM, $Sn_{Zn}$ remains the main

**Table 1**
Photovoltaic parameters calculated for the CZTSe bottom cell in tandem conditions, starting for the baseline and following the various optimizations described in the text. The AM 1.5 efficiency of the CZTSe cell is also shown, along with a target efficiency of the Perovskite top cell for the complete tandem device to reach a 30% efficiency threshold.

| *Condition* | $V_{OC}$ (V) | $J_{SC}$(mA. $cm^{-2}$) | FF (%) | Subcell Eff (%) | AM 1.5 Eff (%) | *Eff. Perovskite for 30% tandem (%)* |
|---|---|---|---|---|---|---|
| #1–2 Baseline 1.56 eV Perovskite | 0.433 | 14.76 | 64.8 | **4.1** | 11.07 | ***25.9*** |
| #1–3 Baseline 1.68 eV Perovskite | 0.444 | 19.19 | 65.3 | **5.6** | 11.07 | ***24.4*** |
| #1–4 Bulk defects red. 1.68 eV top cell | 0.512 | 20.18 | 73.3 | **7.6** | 14.4 | ***22.4*** |
| #1–5 IF defects red. 1.68 eV top cell | 0.518 | 20.24 | 73.4 | **7.7** | 14.7 | ***22.3*** |
| #1–6 BSF 500 nm 1.68 eV top cell | 0.530 | 20.84 | 73.8 | **8.1** | 15.4 | ***21.9*** |
| #1–7 Selec. contacts 1.68 eV top cell | 0.530 | 20.89 | 73.8 | **8.2** | 16.2 | ***21.8*** |

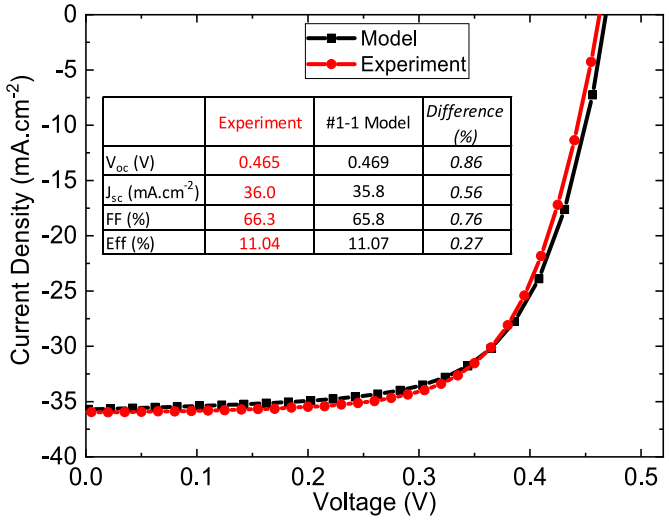


**Fig. 2.** J–V curve comparison between the reference experimental CZTSe cell (red line) and its model mimicry (black line). The corresponding PV figures of merit are shown in the table. (For interpretation of the references to colour in this figure legend, the reader is referred to the Web version of this article.)

performance bottleneck. The reader is invited to verify that statement if deemed necessary using the set of data shared in the supplementary information of this work.

### 3.1.3. Discussion on recombination

The SRH recombination depth profiles in CZTSe are shown Fig. 3, with each of the $n_{-th}$ aforementioned incremental optimizations (solid line) being represented against its n-1 counterpart (dashed line), starting from the baseline CZTSe bottom cell in tandem with a 1.56 eV Perovskite top cell. In each case, the maximum point voltage was chosen ($V_{mpp}$). As expected, reducing the bulk defect density markedly reduces SRH recombination throughout the entire absorber thickness (Fig. 3b), leading to a remarkable improvement in the $V_{oc}$ (68 mV) and a 1 mA $cm^{-2}$ improvement in $J_{sc}$, while no appreciable change is observed when the same is done with interface defects (Fig. 3c). In presence of a back surface field, SRH recombination toward the back interface is markedly reduced, an observation consistent with the increase in $J_{sc}$ (tandem). It should be noted that reducing bulk defects remarkably improves carrier collection under positive bias as illustrated by the jump in FF from 65.3% to 73.3%, as positive external bias reduces the space charge region and a large diffusion length is critical to collect photocarriers. On the other hand, it is trivial to understand why the presence of a BSF does not modify the FF. While not shown here, it should be noted that as mentioned earlier, the BSF-related improvements only exist for an absorber with reduced defect density, as carriers are able to diffuse toward the back interface. The readers may verify by themselves, using the ".scaps" files shared in supplementary materials, that the BSF effectiveness improves as bulk defect density is reduced. This point is also illustrated Fig. S 3 with a simple example. This is in our opinion the main reason why experimental bandgap grading strategies in CZTSe have so far failed to reproduce the success obtained in CIGSe solar cells: it is first and foremost necessary to significantly enhance the carrier diffusion length in CZTSe. In conclusion, it thus appears that the presence of bulk defects is the main bottleneck for CZTSe solar cells. When those are reduced by one order of magnitude and a back surface field is used, the comparatively narrow bandgap of CZTSe allows to reach more than 8% in tandem condition with a Perovskite top cell. For the sake of reference, the CZTSe solar cell efficiency under AM 1.5 illumination would be, in these optimized conditions, 15.4%. We believe such value to be ambitious yet realistic as the current record conversion efficiency recently passed the 13% threshold [3,5,33]. Additionally, the values reported here are very consistent with those recently obtained experimentally on a Perovskite/Kesterite tandem in Ref. [10]. This positions Kesterite absorbers as a promising alternative for bottom cell application free of critical raw materials in tandem devices, with the realistic perspective of performance beyond 30% efficiency.

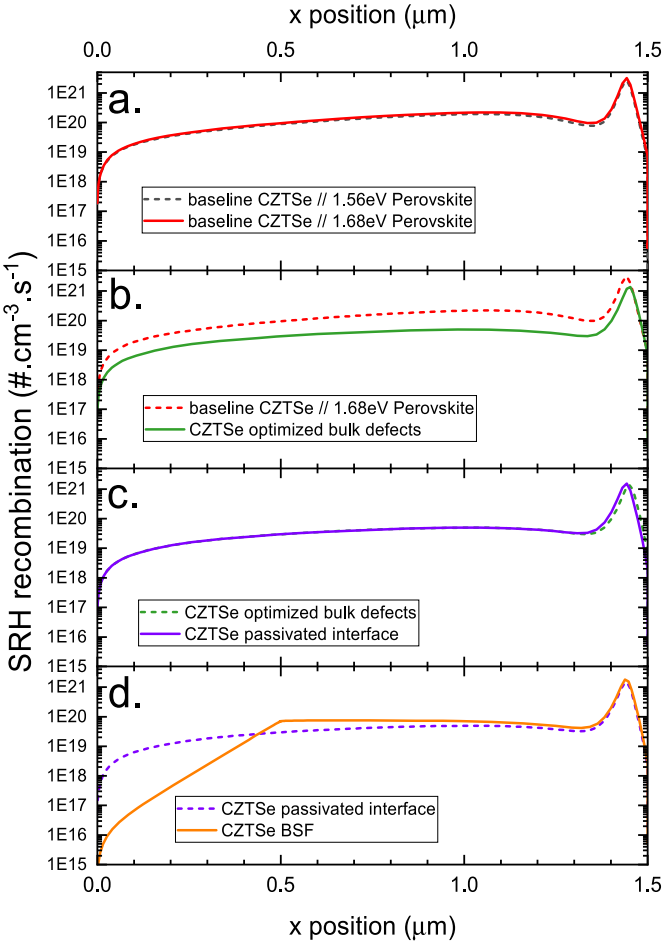


**Fig. 3.** SRH recombination depth profiles corresponding to the various CZTSe configurations described in the text. In each case, the n+1 configuration in represented in solid line against the n-th configuration represented in dashed line.

### 3.2. CZTS/CZGTS as top subcell

We discuss here the feasibility of a tandem device combining a Kesterite top cell with a state-of-the-art crystalline Silicon bottom cell. While such device would forego some of the advantages of working with thin films such as lightweightness and mechanical flexibility, it would also avoid several issues related to the use of Perovskite such as stability and the use of lead, while taking advantage of the reliability and high performance of silicon as bottom subcell. The approach followed is in large part similar to that from the previous part of this work, although in this case, optimization to the performance for the top cell are investigated while the bottom c-Si cell is considered as a fixed entity. The modelled optical transmission of the top Kesterite subcell is used as an input to evaluate the performance of the c-Si bottom cell in tandem conditions.

### 3.2.1. Setting the baseline

Two top cell absorbers are considered: a pure sulfur, CZTS absorber ($E_g \approx 1.6\ eV$) similar to that from Ref. [15], and a pure sulfur CZGTS absorber incorporating germanium with a ratio $\frac{Ge}{(Sn+Ge)} = 0.4$ ($E_g \approx 1.7\ eV$). Note that despite the commonly reported $E_G$ of 1.5 eV, different stoichiometry can be used to tune the band gap of CZTS [34]. The corresponding transmission curves along with the maximum current gain for the bottom cell are shown Fig. 4. Using a wider bandgap material appears critical once again as long as the top cell performance can be preserved, with a maximum gain of nearly 2.6 mA $cm^{-2}$ in current for the bottom Si cell. In the following, only the case of CZGTS will be discussed as optical filter. As compared to the previously discussed Perovskite top cell, the transmission value remains in the 0.6-0.8 range with important interference fringes (perfectly specular interfaces are considered here). It is worth noting that the modelled top cell includes a 115 nm $MgF_2$ anti reflective coating (ARC). This ARC is optimized to minimize the reflectivity over the absorption range of the Kesterite top cell, and therefore results in the slight increase of reflectivity below to Kesterite bandgap as compared to a similar structure without ARC. While transmission is marginally improved without ARC, this does not result in a significantly different current for the Si bottom cell, as the transmission decrease occurs close to the 1.12 eV bandgap of silicon. The influence of a top cell ARC is illustrated in the supplementary information of this work, and particularly in Fig. S 5 where the EQEs of the bottom c-Si cell in tandem conditions are shown for the case of an ARC and without ARC on the top Kesterite cell, along with the corresponding PV parameters of the bottom cell. In each case, the conversion efficiency of the bottom c-Si cell is 8%, which will be taken as a fixed parameter

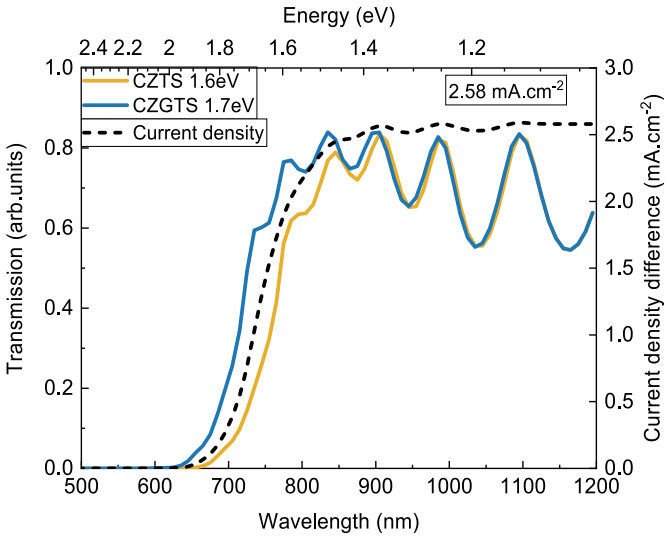


**Fig. 4.** Calculated optical transmissions of the following solar cell stack: $MgF_2$/ITO/ZnO/Kesterite/$MoO_3$/ITO/SLG. The Kesterite bandgaps are 1.6eV (orange line) and 1.7eV (blue line). The dotted line represents the maximum gain in current for the bottom cell calculated by integrating the difference between both transmissions. (For interpretation of the references to colour in this figure legend, the reader is referred to the Web version of this article.)

when calculating the total tandem efficiency in the following section.

We now focus on establishing a baseline for the Kesterite top cell, aiming first at reproducing one of the champion devices developed at our laboratory for pure S Kesterite CZTS [15] developed on transparent FTO substrate (a critical aspect here as the cell is intended for tandem application). Following a similar approach as previously described, and adding interface defects as described in Ref. [24], a baseline is obtained and compared to our experimental reference, as illustrated Fig. 5. The discrepancy between model and experiments is once again low enough on all four main figures of merit for the model to be labelled as quantitative, with a calculated 7.8% conversion efficiency under AM 1.5 illumination. It should nevertheless be stressed that less data were experimentally determined in that case for the experimental reference CZTS as compared to CZTSe; using the shared ".scaps" file in supplementary information, the reader may possibly find minor

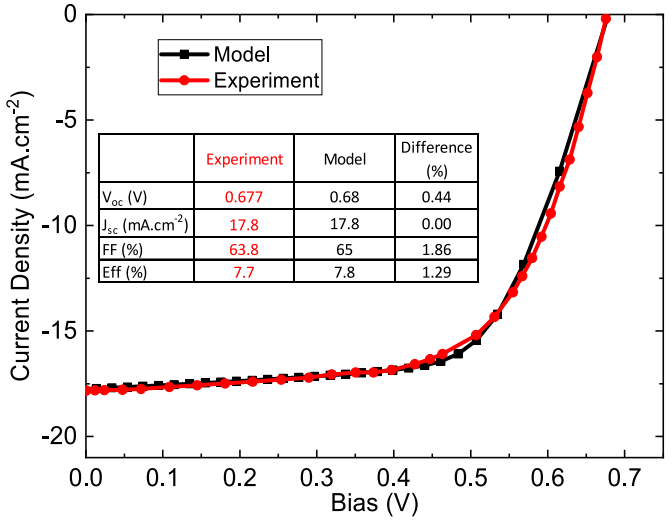


**Fig. 5.** J–V curve comparison between the reference experimental CZTS cell (red line) and its model mimicry (black line). The corresponding PV figures of merit are shown in the table. (For interpretation of the references to colour in this figure legend, the reader is referred to the Web version of this article.)

inconsistencies between parameters, though we have not ourselves and do not expect that the final result should be changed in a significant way.

### 3.2.2. *Tandem performance and incremental optimizations*

Starting from this 7.8% efficient baseline model, the total tandem efficiency in combination with a c-Si bottom cell is calculated to be 15.9%, as shown Table 2. It should however be stressed that the transmission values calculated for the Kesterite top cell assume a transparent $MoO_3$ interlayer at the back interface even though a less transparent $MoS_2$ interlayer was likely formed in the reference cell from Ref. [15]. Transparent transition metal oxides as hole transport layers are an active field of study in the community of chalcogenide cells and we recently reported on the necessity to use those rather than $Mo(S,Se)_2$ for tandem application [17], and we thus assumed an optically optimum configuration for the Kesterite top cell here. The complex optical indices of both $MoO_3$ and $MoS_2$ are shared in the supplementary information of this work for the interested reader to make the calculation replacing the first by the second.

Incremental optimizations to the Kesterite CZTS top cell are presented in Table 2. Contrarily to case of Se-Kesterite, where the performance bottleneck is ascribed to bulk defects in the literature and confirmed by the first part of this work, wide bandgap Kesterite are often limited at the CZTS/CdS interface as recently reported in the work of Li et al. [24]. The authors suggest acceptor–like interface defects, band misalignment and improper surface doping profile as the main factors hampering conversion efficiency. This work will discuss the first two aspects, while the third one is addressed by combining experiments and modelling in an upcoming study to be released shortly following this one, and of which a pre-version is available [35]. Optimizing the band alignment by substituting Cd with Zn is a straightforward approach to reduce the electron affinity of the buffer layer and match the bands of the p and n region at $\chi = 4.0\ eV$. This permits to remarkably increase the $V_{OC}$ from 0.68 V to 0.88 V (with modest increases in current and FF as well), resulting in single cell efficiency of 10.8% and a total tandem efficiency of 18.8%. Reducing the interface defect density by 1 OM, following for example a process similar to that reported by our group in Ref. [36], results in a further increase of the efficiency by an absolute 0.5 point; however, the reader may verify on their own that reducing interface defects alone without improving the interface band matching does lead to a more significant relative improvement as compared to the baseline ($\eta = 9.22\%$). This observation confirms that both approaches address a similar limitation of the device [24] which was much less problematic for CZTSe solar cells. Furthermore, reducing the bulk defect density once again allows for a significant efficiency boost up to 13.6% (21.7% tandem), which goes in a direction similar to that of reference [2] where bulk defects are also identified as a major bottleneck for this technology. Finally, for reasons similar to those detailed in the comments of Table 1, a back surface field strategy with bandgap grading

**Table 2**
Photovoltaic parameters calculated for the CZTS top cell in tandem conditions, starting for the baseline and following the various optimizations described in the text. It should be noted that the tandem efficiencies are in the hypothesis of a 1.7eV absorber, that is with Ge alloying.

| Condition | $V_{oc}$ (V) | $J_{sc}$ (mA. $cm^{-2}$) | FF (%) | Eff (%) | Tandem Eff (%) |
|---|---|---|---|---|---|
| *c-Si AM1.5* | *0.70* | *38.3* | *84.7* | *22.9* | - |
| *c-Si bottom cell (1.7 eV top cell)* | *0.68* | *14.0* | *84.2* | *8.05* | - |
| #2-1 Baseline | 0.68 | 17.7 | 65.1 | 7.8 | ***15.9*** |
| #2-2 Optimized buffer $(Cd_{0.5},Zn_{0.5})S$ | 0.88 | 18.5 | 66.3 | 10.8 | ***18.8*** |
| #2–3 IF defects red. | 0.93 | 18.6 | 65.4 | 11.3 | ***19.4*** |
| #2–4 Bulk defects red. | 0.99 | 19.6 | 70.3 | 13.6 | ***21.7*** |
| #2–5 Back contact optimization | 1.00 | 20.8 | 70.6 | 14.7 | ***22.7*** |
| #2–6 Select. contacts | 1.03 | 21.3 | 80.2 | 17.7 | ***25.7*** |

becomes relevant once the material's bulk properties are improved and the single cell efficiency is markedly improved up to 14.7% (22.7% tandem). The ideal case of perfectly selective contacts is also shown as an upper limit target, with a single cell efficiency of 17.7% (25.7% tandem). This tends to show that carrier extraction is, in this case, more critical than it was in the case of an optimized CZTSe.

As one can see, and despite numerous ambitious optimizations, the total tandem efficiency remains well below the detailed balance limit and can barely approach the single cell efficiency of the best c-Si devices. In that context, and with Perovskite or even CdTe solar cells already covering a bandgap range compatible with a c-Si bottom subcell, the use of Kesterite as top cell appears difficult to justify despite the material's numerous advantages, unless a performance breakthrough at single cell level not accounted here was to happen.

### 3.2.3. Discussion on recombination rate

The SRH recombination depth profile for each of the considered configurations of the Kesterite top cell at $V_{mpp}$ is presented Fig. 6. Comparing 6a, 6b and 6c allows to clearly visualize the decoupling between the two interface optimizations and the bulk defects optimization. While all three configurations lead to a sizeable improvement unlike CZTSe, the first recombination profile being affected is expectedly the one corresponding to a reduction in bulk defect density (Fig. 6c) with a homogenous decrease in SRH recombination, despite the fact that

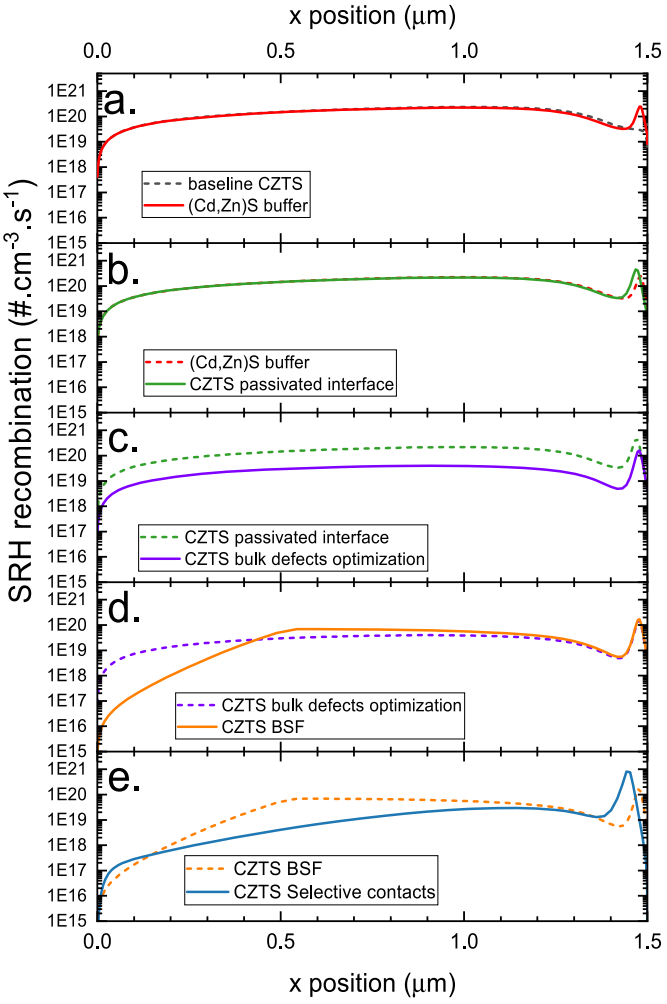


**Fig. 6.** SRH recombination depth profiles corresponding to the various CZTS configurations described in the text. In each case, the n+1 configuration in represented in solid line against the n-th configuration represented in dashed line.

(a) and (b) correspond to a similar increase in $J_{sc}$ as (c) of about 1 mA $cm^{-2}$. When looking at the evolution of the FF however, we see that improving the CZTS/CdS interface (Fig. 6a and b) does not lead to a significant change compared to the baseline and it remains at about 65%. On the other hand, the reduction in bulk defect density (Fig. 6c) markedly improves the FF to more than 70%, which is consistent with the observed decrease SRH recombination at $V_{mpp}$. While interfaces are often pointed out as critical in wide bandgap Kesterite [24] and for good reasons, reducing bulk defects appears once again to be the main priority if this technology is to become a relevant player in the future of chalcogenide solar cells and particularly in the ever-growing tandem device landscape. Once again, the increase in carrier diffusion length permits to significantly enhance the beneficial effect of the BSF (Fig. 6d), with a steep decline in SRH recombination at the vicinity of the back contact; this effect is independent from the applied external voltage, which explains why the FF is here unaffected. In the ideal case of perfectly selective front and back electrodes, the opposite is observed with a moderate increase in $J_{sc}$ while the FF jumps to 80%; the latter point can be easily understood when observing the band diagram: in the absence of a space charge region, the carrier collection depends more on the diffusion current rather than the drift and is thus marginally affected by the applied voltage. One can verify using the data shared in supplementary information that the difference in SRH recombination between case #2–5 and #2–6 is much more visible at $V_{mpp}$ than it is in zero bias conditions.

### 3.3. Limitations, perspectives and take-home message

The simulations presented here are claimed to be quantitative, and their accurate reproduction of all four main figures of merit of a solar cell while using a consistent set of experimental parameters (that is, from sample produced from one single experimental process) supports such claim. This could nevertheless be disputed on several accounts based on inherent limitations to our approach. Chiefly, as SCAPS was used for the electrical part, no 2D effects are taken into account and the presence of grain boundaries would have to be considered for a more accurate representation of the system. It is however possible that the diffusion of alkali elements during fabrication would passivate the grain boundaries [37,38], rendering the unidimensional approach chosen here sufficient for describing Kesterite solar cells. Our group has not been able to reach, so far, a definitive conclusion about the influence of grain boundaries on the performance Kesterite solar cells. Moreover, the macroscopic material parameters used here and experimentally determined by our group on thin-films already factor in the possible influence of the grain boundaries. Using a 2D simulation approach would nevertheless be a straightforward improvement pathway to this study.

The robustness of our two baselines and the optical modelling would need to be assessed against other experimental devices. We have done so in the supplementary information to this work by creating a mimicry of the CZTSe solar cell reported in Ref. [10]. By only varying the bulk defect concentration, we were able to simultaneously reproduce all four PV figures of merit from this separate study with an excellent accuracy. Additionally, the measured tandem performance ($\eta = 3.85\%$) was also accurately reproduced by our model when using a 1.65 eV Perovskite top cell (modelled $\eta = 4.0\%$)). More investigations are of course needed, but this specific case is an example of the reliability of the set of parameters shared in this work, which the community is encouraged to assess against their own experimental devices.

The influence of the doping profile in Kesterite is not considered in this study. Our recent experimental results suggest that a depth-controlled carrier density can lead to a measurable improvement in PV performance, which we have been able to confirm using numerical modelling. A pre-version of the corresponding study can be found in Ref. [35], where the CZTSe baseline used is similar to that presented in this work.

While our code permits to take into account light scattering effects,

following the Beckmann-Spizzichino model [39], we decided against it as fabricating specular surfaces and interfaces is a requirement if aiming for a tandem application. This is for instance a central point of optimization in a recently published study on Perovskite/Kesterite tandem [10]. Several methods exist to significantly reduce the surface roughness of Kesterite films, among which $Br_2$ chemical etching [40] is possibly the most straightforward. As a result, it appears sensible to only consider specular interfaces in this work and ignore light scattering effects.

An important limitation of this work exists when modelling wide $E_g$ Kesterite. We accurately reproduced the behavior of our reference pure sulfur CZTS device; however, we also argue that it is necessary to increase the bandgap of the film for a tandem with c-Si by substituting 40% of Sn by Ge, and we report on the performance of the c-Si bottom cell in such conditions. As our group has not yet fabricated such Kesterite composition, we do not yet possess a consistent set of experimentally determined material parameters and only CZTS excluding Ge was electrically modelled. This discrepancy is not a fundamental flaw of the method, but possible performance enhancements (or diminution) from the incorporation of Ge to the wide bandgap Kesterite film are not factored in.

Finally, the case of a Kesterite-Kesterite tandem device is not discussed here, as deemed beyond the scope of this work considering the present state of the art. Nevertheless, the interested reader may carry out such study using the data shared in the supplementary information of this manuscript.

The important points developed in this work are the following:

- A modelling baseline of both CZTS and CZTSe is proposed and shared with the community, using the popular simulation tool SCAPS. Those baselines where obtained to mimic the cells developed by our group and do so in a realistic, quantitative manner, and we believe that the data shared here can be readily used and possibly improved upon in the future. If so, we would encourage other groups to also make all data available for the community.
- When combining electrical modelling by SCAPS with a quantitative optical modelling using the transfer matrix approach, it is possible to offer an overview of the potential of Kesterite both as a bottom cell (with Perovskite as top cell) and as a top cell (with c-Si as bottom cell).
- It is found that a moderate improvement of Selenium Kesterite CZTSe would make this material a realistic contender as bottom cell; indeed, its narrow 1.04eV bandgap is a significant advantage over the wider bandgap materials c-Si and CIGSe, which permits to partly offset the performance deficit of Kesterite. As an example, it is found that a 15.4% CZTSe combined with a 22% Perovskite would approach and possibly reach the detailed balance limit of a single junction.
- Despite several ambitious optimizations being considered here, the performance deficit of wide bandgap Kesterite as compared to Perovskite or CdTe appears too wide to envision a short to middle term application of this technology, unless an important breakthrough is made in the upcoming years.

## 4. Conclusion

By means of numerical modelling using simple tools and decoupling optical and electrical simulation, the potential of the Kesterite family of photovoltaic absorbers was assessed in quantitative manner. Using a consistent set of experimentally determined material and device parameters, a pure-Se narrow bandgap Kesterite (bottom subcell) and a pure-S wide bandgap Kesterite (top subcell) were reproduced in an accurate manner, with $\lesssim$1% of discrepancy in all four solar cell parameters simultaneously. From those two baselines and using the transfer matrix method for optical modelling, 4T tandem performance with a Perovskite top cell, or with a c-Si bottom cell, were respectively estimated. By implementing optimizations based on some of the current dominant research lines investigated by the Kesterite community, improved designs were proposed for both the narrow and wide bandgap Kesterite cells and their performance in tandem conditions were assessed. It is found that for a narrow bandgap Kesterite cell used as bottom subcell in combination with a Perovskite top cell, and a moderate increase of the efficiency beyond the current state of the art would be sufficient to consider Kesterite as a credible option, as a bottom cell efficiency of 8% is feasible by combining a reduction of the bulk defect density with a back surface field (15.4% AM 1.5). For the case of a wide bandgap Kesterite combined with a c-Si bottom cell, a similarly ambitious set of optimizations yields tandem performance which remain below the state of the art of a single junction c-Si, and the performance threshold for Kesterite to be a viable top cell in a tandem design appears difficult to reach at short or middle term without a significant breakthrough. It will be up to the community to find the merits of pursuing such breakthrough.

Beyond the results reported here, this work also offers an extensive, consistent and reliable set of data for the community to both use and assess in their modelling work. All optical data and material parameters are made available, which will hopefully contribute positively to the research on Kesterite solar cells as a whole, offering a reliable baseline allowing a straightforward comparison in the results reported by different groups.

## CRediT authorship contribution statement

**Alex Jimenez-Arguijo:** Writing – review & editing, Investigation, Data curation. **Axel Gon Medaille:** Writing – review & editing, Methodology, Data curation. **Alejandro Navarro-Güell:** Writing – review & editing, Data curation. **Maykel Jimenez-Guerra:** Methodology. **Kunal J. Tiwari:** Writing – review & editing, Methodology, Investigation. **Marcel Placidi:** Resources, Project administration. **Moleko Samuel Mkehlane:** Investigation. **Emmanuel Iwuoha:** Validation, Supervision. **Alejandro Perez-Rodriguez:** Supervision. **Edgardo Saucedo:** Supervision. **Sergio Giraldo:** Writing – review & editing, Supervision, Data curation. **Zacharie Jehl Li-Kao:** Writing – review & editing, Writing – original draft, Supervision, Methodology, Investigation, Formal analysis, Data curation, Conceptualization.

## Declaration of competing interest

The authors declare that they have no known competing financial interests or personal relationships that could have appeared to influence the work reported in this paper.

## Data availability

Data will be made available on request.

## Acknowledgements

This project has received funding from the European Union's Horizon 2020 research and innovation programme under grant agreement No. 952982 (CUSTOM-ART) and under grant agreement No. 777968 (INFINITE-CELL), and from the R + D + i Cell2Win project Ref. PID 2019-104372RB-C31 funded by MCIN/AEI/10.13039/5011000110033. Authors from IREC belong to the SEMS (Solar Energy Materials and Systems) Consolidated Research Group of the "Generalitat de Catalunya" (Ref. 2017 SGR 862)". M.P. acknowledges the financial support from Spanish Ministry of Science, Innovation and Universities within the Ramón y Cajal (RYC-2017–23758) program. ES also thanks the ICREA academia program.

## Appendix A. Supplementary data

Supplementary data to this article can be found online at https://doi.

org/10.1016/j.solmat.2022.112109.

## References


[1] S.N. Hood, et al., Status of materials and device modelling for kesterite solar cells, J. Phys.: Energy 1 (4) (2019), 042004.

[2] S. Kim, J.A. Márquez, T. Unold, A. Walsh, Upper limit to the photovoltaic efficiency of imperfect crystals from first principles, Energy Environ. Sci. 13 (5) (2020) 1481–1491, https://doi.org/10.1039/D0EE00291G.

[3] Y. Gong, et al., Elemental de-mixing-induced epitaxial kesterite/CdS interface enabling 13%-efficiency kesterite solar cells, Nat. Energy 7 (10) (Oct. 2022), https://doi.org/10.1038/s41560-022-01132-4. Art. no. 10.

[4] A. Jimenez-Arguijo, et al., Small atom doping: a synergistic strategy to reduce SnZn recombination center concentration in Cu2ZnSnSe4? Solar RRL (2022) https://doi.org/10.1002/solr.202200580.

[5] M.A. Green, et al., Solar cell efficiency tables (Version 60), Progress Photovoltaics 30 (7) (Jul. 2022) 687–701, https://doi.org/10.1002/pip.3595.

[6] National Renewable Energy Laboratory (NREL), Best research-cell efficiency chart. https://www.nrel.gov/pv/cell-efficiency.html. (Accessed 30 August 2022).

[7] A. Al-Ashouri, et al., Monolithic perovskite/silicon tandem solar cell with >29% efficiency by enhanced hole extraction, Science 370 (6522) (Dec. 2020) 1300–1309, https://doi.org/10.1126/science.abd4016.

[8] M. Nakamura, K. Yamaguchi, Y. Kimoto, Y. Yasaki, T. Kato, H. Sugimoto, Cd-free Cu(In,Ga)(Se,S)2 thin-film solar cell with record efficiency of 23.35, IEEE J. Photovoltaics 9 (6) (Nov. 2019) 1863–1867, https://doi.org/10.1109/JPHOTOV.2019.2937218.

[9] First Solar, First Solar achieves yet another cell conversion efficiency world record. https://investor.firstsolar.com/news/press-release-details/2016/First-Solar-Achieves-Yet-Another-Cell-Conversion-Efficiency-World-Record/default.aspx, Feb. 23, 2016.

[10] S.K. Hwang, I.J. Park, S.W. Seo, J.H. Park, S.J. Park, J.Y. Kim, Electrochemically Deposited CZTSSe Thin Films for Monolithic Perovskite Tandem Solar Cells with Efficiencies over 17%, Energy & Environmental Materials, 2022, e12489 https://doi.org/10.1002/eem2.12489.

[11] J. Lin, et al., Optoelectronic simulation of four-terminal all-inorganic CsPbI3/CZTSSe tandem solar cell with high power conversion efficiency, *Phys. Chem. Chem. Phys.*, Aug (2022), https://doi.org/10.1039/D2CP02302D.

[12] D. Jayan K, "Theoretical Modeling of Perovskite–Kesterite Tandem Solar Cells for Optimal Photovoltaic Performance," Energy Technology, no. n/a, p. 2200635, doi: 10.1002/ente.202200635.

[13] M. Burgelman, P. Nollet, S. Degrave, Modelling polycrystalline semiconductor solar cells, Thin Solid Films 361–362 (Feb. 2000) 527–532, 16/S0040-6090(99)00825-1.

[14] S. Giraldo, et al., How small amounts of Ge modify the formation pathways and crystallization of kesterites, Energy Environ. Sci. 11 (3) (2018) 582–593, https://doi.org/10.1039/C7EE02318A.

[15] E. Ojeda-Durán, et al., High efficiency Cu2ZnSnS4 solar cells over FTO substrates and their CZTS/CdS interface passivation via thermal evaporation of Al2O3, J. Mater. Chem. C 9 (16) (Apr. 2021) 5356–5361, https://doi.org/10.1039/D1TC00880C.

[16] M. Gloeckler, A.L. Fahrenbruch, J.R. Sites, Numerical modeling of CIGS and CdTe solar cells: setting the baseline, Proc. 3rd World Conf. Photovoltaic Energy Conversion 1 (2003) 491–494, mai 2003, vol. 1.

[17] K.J. Tiwari, et al., Feasibility of a full chalcopyrite tandem solar cell: a quantitative numerical approach, Solar RRL 5 (7) (2021), 2100202, https://doi.org/10.1002/solr.202100202.

[18] M. Jeong, et al., Stable perovskite solar cells with efficiency exceeding 24.8% and 0.3-V voltage loss, Science 369 (6511) (Sep. 2020) 1615–1620, https://doi.org/10.1126/science.abb7167.

[19] Z. Xie, et al., Refractive index and extinction coefficient of NH2CH= NH2PbI3 perovskite photovoltaic material, J. Phys. Condens. Matter 29 (24) (2017), 245702.

[20] S. Sarkar, et al., Hybridized guided-mode resonances via colloidal plasmonic self-assembled grating, ACS Appl. Mater. Interfaces 11 (14) (2019) 13752–13760.

[21] M. Filipič, et al., CH 3 NH 3 PbI 3 perovskite/silicon tandem solar cells: characterization based optical simulations, Opt Express 23 (7) (2015) A263–A278.

[22] Y. Xu, J.-H. Yang, S. Chen, X.-G. Gong, Defect-assisted nonradiative recombination in Cu 2 ZnSn Se 4 : a comparative study with Cu 2 ZnSn S 4, Phys. Rev. Materials 5 (2) (Feb. 2021), 025403, https://doi.org/10.1103/PhysRevMaterials.5.025403.

[23] J. Li, Z.-K. Yuan, S. Chen, X.-G. Gong, S.-H. Wei, Effective and noneffective recombination center defects in Cu $_2$ ZnSnS $_4$ : significant difference in carrier capture cross sections, Chem. Mater. 31 (3) (Feb. 2019) 826–833, https://doi.org/10.1021/acs.chemmater.8b03933.

[24] J. Li, et al., Interface recombination of Cu2ZnSnS4 solar cells leveraged by high carrier density and Interface defects, Solar RRL 5 (10) (2021), 2100418, https://doi.org/10.1002/solr.202100418.

[25] R. Fonoll-Rubio, et al., Characterization of the stability of indium tin oxide and functional layers for semitransparent back-contact applications on Cu(in,Ga)Se2 solar cells, Solar RRL 6 (7) (2022), 2101071, https://doi.org/10.1002/solr.202101071.

[26] X. Liu, et al., Highly efficient wide-band-gap perovskite solar cells fabricated by sequential deposition method, Nano Energy 86 (Aug. 2021) 106114, https://doi.org/10.1016/j.nanoen.2021.106114.

[27] Z. Li, et al., Minimized surface deficiency on wide-bandgap perovskite for efficient indoor photovoltaics, Nano Energy 78 (Dec. 2020) 105377, https://doi.org/10.1016/j.nanoen.2020.105377.

[28] S. Gharibzadeh, et al., Record open-circuit voltage wide-bandgap perovskite solar cells utilizing 2D/3D perovskite heterostructure, Adv. Energy Mater. 9 (21) (Jun. 2019), https://doi.org/10.1002/aenm.201803699. Art. no. 21.

[29] M.A. Mahmud, et al., Cation-diffusion-based simultaneous bulk and surface passivations for high bandgap inverted perovskite solar cell producing record Fill factor and efficiency, Adv. Energy Mater. (Aug. 2022), 2201672, https://doi.org/10.1002/aenm.202201672.

[30] J. Andrade-Arvizu, et al., Rear band gap grading strategies on Sn-Ge-alloyed kesterite solar cells, ACS Appl. Energy Mater. 3 (11) (Nov. 2020) 10362–10375, https://doi.org/10.1021/acsaem.0c01146.

[31] J. Andrade-Arvizu, "Band Gap Grading Strategies for High Efficiency Kesterite Based Thin Film Solar Cells," University of Barcelona.

[32] S. Padhy, R. Mannu, U.P. Singh, Graded band gap structure of kesterite material using bilayer of CZTS and CZTSe for enhanced performance: a numerical approach, Sol. Energy 216 (Mar. 2021) 601–609, https://doi.org/10.1016/j.solener.2021.01.057.

[33] J. Li, et al., Defect control for 12.5% efficiency Cu $_2$ ZnSnSe $_4$ kesterite thin-film solar cells by engineering of local chemical environment, Adv. Mater. 32 (52) (Dec. 2020), 2005268, https://doi.org/10.1002/adma.202005268.

[34] C. Malerba, CZTS stoichiometry effects on the band gap energy, J. Alloys Compd. 7 (2014), https://doi.org/10.1016/j.jallcom.2013.07.199.

[35] A.J. Arguijo, Z.J. Li-Kao, E. Saucedo, S. Giraldo, Innovative post-deposition treatment for local doping control in Cu2ZnSnSe4 by a combined temperature-voltage method, Zenodo (Sep. 2022), https://doi.org/10.5281/zenodo.7128898.

[36] E. Ojeda-Durán, et al., CZTS solar cells and the possibility of increasing VOC using evaporated Al2O3 at the CZTS/CdS interface, Sol. Energy 198 (Mar. 2020) 696–703, https://doi.org/10.1016/j.solener.2020.02.009.

[37] J. Kim, et al., Sodium-assisted passivation of grain boundaries and defects in Cu $_2$ ZnSnSe $_4$ thin films, Phys. Chem. Chem. Phys. 22 (14) (2020) 7597–7605, https://doi.org/10.1039/C9CP06537G.

[38] W.-J. Yin, Y. Wu, S.-H. Wei, R. Noufi, M.M. Al-Jassim, Y. Yan, Engineering grain boundaries in Cu $_2$ ZnSnSe $_4$ for better cell performance: a first-principle study, Adv. Energy Mater. 4 (1) (Jan. 2014), https://doi.org/10.1002/aenm.201300712. Art. no. 1.

[39] P. Beckmann, A. Spizzichino, The scattering of electromagnetic waves from rough surfaces, Accessed: Dec. 10, 2021. [Online]. Available: https://ui.adsabs.harvard.edu/abs/1987ah...book.....B, 1987.

[40] K.J. Tiwari, et al., Defect depth-profiling in kesterite absorber by means of chemical etching and surface analysis, Appl. Surf. Sci. 540 (Feb. 2021), 148342, https://doi.org/10.1016/j.apsusc.2020.148342.